Modeling the free energy surfaces of electron transfer in condensed phases

Dmitry V. Matyushov[a] and Gregory A. Voth
Department of Chemistry and Henry Eyring Center for Theoretical Chemistry, University of Utah, 315 South 1400 East, Salt Lake City, Utah 84112-0850

(Received 18 May 2000; accepted 6 July 2000)

We develop a three-parameter model of electron transfer (ET) in condensed phases based on the Hamiltonian of a two-state solute linearly coupled to a harmonic, classical solvent mode with different force constants in the initial and final states (a classical limit of the quantum Kubo–Toyozawa model). The exact analytical solution for the ET free energy surfaces demonstrates the following features: (*i*) the range of ET reaction coordinates is limited by a one-sided fluctuation band, (*ii*) the ET free energies are infinite outside the band, and (*iii*) the free energy surfaces are parabolic close to their minima and linear far from the minima positions. The model provides an analytical framework to map physical phenomena conflicting with the Marcus–Hush two-parameter model of ET. Nonlinear solvation, ET in polarizable charge-transfer complexes, and configurational flexibility of donor-acceptor complexes are successfully mapped onto the model. The present theory leads to a significant modification of the energy gap law for ET reactions. © *2000 American Institute of Physics.* [S0021-9606(00)50937-4]

I. INTRODUCTION

The activation barrier of electron transfer (ET) reactions is formed by the free energy invested to create the resonance of the instantaneous energies E_i of the initial $(i=1)$ and final $(i=2)$ states. The energies E_i, depending on the instantaneous nuclear configuration, are derived by tracing out the electronic degrees of freedom in the system density matrix.[1–3] Correspondingly, the energy gap $\Delta E=E_2-E_1$ is commonly defined as the collective mode

$$X=\Delta E \tag{1}$$

driving ET.[4–8] The probability of realization of a particular instantaneous energy gap X is found by tracing out the solvent coordinates at a fixed magnitude of X. This reduced description results in the diabatic *free energies* of ET along X given by the constrained trace

$$e^{-\beta F_i(X)+\beta F_{0i}}=\beta^{-1}\langle\delta(\Delta E-X)\rangle_i. \tag{2}$$

Here $\beta=1/k_BT$,

$$\langle\ldots\rangle_i=\mathrm{Tr}\,(\ldots e^{-\beta E_i}/\mathrm{Tr}(e^{-\beta E_i}),) \tag{3}$$

and the nuclear degrees of freedom of the solvent are traced out in Eq. (2); F_{0i} is the equilibrium free energy of the ET system in its ith electronic state.

The classical model of a two-state solute linearly coupled to a harmonic solvent which effective force constant does not change with electronic transitions[4,9] presents perhaps the only exact, closed-form solution for $F_i(X)$ available to date in the field of ET. The combination of its classical limit for the solvent nuclear modes (Marcus–Hush theory)[10] with its quantum limit[11] for intramolecular skeletal vibrations is commonly used to treat the reaction kinetics, the dependence of the ET rate on the the equilibrium energy gap $\Delta F_0=F_{02}-F_{01}$ (energy gap law), or to generate optical bandshapes.[11(c),12] Two regions of the energy gap law are usually distinguished. For relatively small activation barriers, a parabolic energy gap law results from the Gaussian distribution of the solvent nuclear fluctuations.[10] This behavior is a manifestation of the well-known ''law of intersecting parabolas'' in the standard ET theory. Multiphonon vibrational excitations provide a more effective activation channel for larger barriers generating a linear-logarithmic, $\propto|\Delta F_0|\ln(|\Delta F_0|)$, dependence of the activation barrier on the equilibrium energy gap ΔF_0.[11(c)] This vibrational mechanism is currently applied to explain the linear energy gap law observed for large values of the free energy gap.[11(c),12,13]

Since the earliest days of the theory of radiationless transitions a possibility of a bilinear solute–solvent coupling has been considered.[14–17] This problem is isomorphic to that of a solute linearly coupled to a solvent mode with the force constants different in the initial and final electronic states (Duschinsky rotation of normal modes[17]). Throughout this article, we will refer to this model as the Q-model (quadratic coupling) contrasting it to the L-model (linear coupling) embodied in the Marcus–Hush (MH)[10] theory of ET. (The latter assumes the linear coupling to the nuclear driving mode with equal force constants in the two electronic states.) Although a general solution of the Q-model was given by Kubo and Toyozawa,[14] its quantum limit does not allow a closed-form analytical representation for $F_i(X)$.[18] The model hence has not received wide application to ET reactions. Instead, nonlinear solute–solvent coupling has been modeled by two displaced *free energy* parabolic surfaces $F_i(X)$ with different curvatures.[19,20] This model, advanced by Kakitani and

[a]Present address: Department of Chemistry and Biochemistry, Arizona State University, P.O. Box 871604, Tempe, AZ 85287-1604. Electronic mail: dmitrym@asu.edu

TABLE I. Mapping of the Q-model on simulation data for charge separation reactions (energies are in kcal/mol).

Solvent	$\hbar\Delta\omega_{st}$[a]	λ_1	λ_2	α_1	γ	Reference
Lattice of point dipoles	157	121.1	48.3	2.82	1.01	25
Polar liquid	50	27.0	17.4	7.04	1.04	20
Polar liquid	267	231.5	67.1	2.03	1.04	23a
Water	421	164.4	181.2	−35.8	0.99	23b

[a]$\hbar\Delta\omega_{st}=\langle X\rangle_1-\langle X\rangle_2$.

Mataga, was used to represent nonlinear solvation effects on the ET energy gap law.[19] Tachiya criticized that approach, arguing that nonlinear effects should result in asymmetric surfaces $F_i(X)$ with equal curvatures at each given value of X.[21] The latter argument is based on the fact that the two diabatic free energy surfaces are coupled by the linear relation[5–8,22–24]

$$F_2(x)=F_1(X)+X, \tag{4}$$

as first established by Warshel.[5(a)] The relation is based on the transformation of the constrained trace as

$$\langle\delta(X-\Delta E)\rangle_2=e^{\beta(\Delta F_0-X)}\langle\delta(X-\Delta E)\rangle_1. \tag{5}$$

In this article we reexamine the problem of nonlinear solute–solvent coupling in application to modeling the ET free energy surfaces in condensed phases. Two major shortcomings of the earlier studies of this problem can be identified. First, there is no analytic, closed-form solution for the free energies that (*i*) derives from the system Hamiltonian according to Eq. (2), (*ii*) includes nonlinear effects, and (*iii*) complies with the linear constraint in Eq. (4). The absence of such a solution hampers construction of global free energy surfaces from limited data provided by computer simulations or spectroscopic experiments. In addition, the parabolic MH representation often does not provide enough flexibility to use it in the bandshape analysis of asymmetric optical bands. Second, most simulation studies of nonlinear solvation effects have been performed on a variety of systems with different solute geometries and various solvation environments including fluids, glasses, and lattices. As a result, nonlinear solvation effects ranging from vanishingly small[5] to very substantial[20,25] have been reported (see also Table I). As no systematic studies for different phase states of the solvent for the same charge-transfer (CT) system have been performed, it remains unclear for which solute geometries and solvent environments the nonparabolic free energy surfaces should manifest themselves and whether these nonlinear effects allow for a description in terms of an analytical model.

As a development toward solving the first problem, the well-known model of a two-state solute linearly coupled to a classical, collective solvent mode whose force constants differ in the two electronic states is considered. Instead of assuming the parabolic form for $F_i(X)$,[19] in Sec. II, we derive the nonparabolic free energy surfaces of ET by applying Eq. (2). An exact solution for $F_i(X)$ is obtained. The free energy surfaces are asymmetric and Eq. (4) is found to hold provided the solvent mode driving ET is thermodynamically stable (Sec. III). The region where the free energy surfaces have finite values and Eq. (4) holds is, however, limited to a one-sided band of the reaction coordinates; the free energies $F_i(X)$ are infinite beyond this one-sided band. The model predicts quadratic or linear free energy surfaces depending on the model parameters. Furthermore, quadratic and linear energy gap laws hold for transitions driven by a purely classical nuclear mode without invoking quantum vibrations.[11]

The analytical model developed here can be used for treating real systems or mapped onto computer simulations. The model parameters are defined through the two first cumulants of the energy gap reaction coordinate X that correspond to spectral moment measured by optical spectroscopy (Sec. IV). Several model systems used to study nonlinear solvation in molecular solvents can be successfully mapped onto the Q-model (Sec. V A). In order to study nonlinear solvation effects, reaction coordinate cumulants are simulated here for a dipolar solute in a hard sphere dipolar, polarizable and nonpolarizable, media which form liquid and solid phases. These cumulants are used to construct global, nonequilibrium free energy surfaces provided by the analytical solution. The analytical free energy surfaces agree well with those directly extracted from simulations.

The nonlinear equilibrium *solvation* effects[26] are usually relatively moderate for dense liquid solvents,[5,6,22,23(b),27,28] implying that the Gaussian approximation holds well for the classical collective solvent mode driving ET.[29,30] It does not, however, mean that parabolic free energy surfaces should be the rule for condensed phase ET. We show here that intramolecular *solute* modes, both electronic[3,31] and nuclear, when coupled to a Gaussian solvent mode generate a nonlinear solute–solvent coupling. A bilinear coupling characterizes ET in polarizable CT complexes as well as the modulation of the solute–solvent potential by configurational changes of the donor–acceptor complex. Both effects can be mapped onto the Q-model, as is shown in Secs. V B and V C. Finally, conclusions are drawn in Sec. VI.

II. FREE ENERGY SURFACES OF ET

Consider two electronic states of an ET complex linearly coupled to a harmonic, collective solvent mode q with the force constant κ_i changing with electronic excitation[14]

$$E_i=I_i-C_iq+\tfrac{1}{2}\kappa_iq^2. \tag{6}$$

Here I_i is the electronic energy composed of the vacuum electronic energy and the solvation free energy from the solvent electronic degrees of freedom. The parameter C_i defines the strength of the solute–solvent coupling. The collective coordinate q driving the electronic transition can be pro-

jected out from the microscopic liquid Hamiltonian or represented as a linear combination of harmonic degrees of freedom characterized by a spectral density.[32]

The δ-function in Eq. (2) should be understood as the Fourier integral

$$e^{-\beta F_i(X)+\beta F_{0i}}=\int_{-\infty}^{\infty}\frac{d\xi}{2\pi}e^{i\xi\beta X}\mathrm{Tr}(e^{-i\xi\beta\Delta E-\beta E_i}) /\mathrm{Tr}(e^{-\beta E_i}). \quad (7)$$

The traces in the above equation reduce to integration over q yielding

$$e^{-\beta F_i(X)+\beta F_{0i}}=\int_{-\infty}^{\infty}\frac{d\xi}{2\pi}\sqrt{g_i(\xi)}\exp[\mathcal{F}_i(\xi,X)]. \quad (8)$$

Here,

$$F_{0i}=I_i-C_i^2/2\kappa_i. \quad (9)$$

is the equilibrium free energy in the ith state,

$$g_i(\xi)=(1+i\xi\Delta\kappa/\kappa_i)^{-1}, \quad (10)$$

and

$$\mathcal{F}_i(\xi,X)=i\xi\beta(X-X_0)-\beta\xi\lambda_i\alpha_i^2(\xi-i\alpha_i)^{-1}. \quad (11)$$

The function $\mathcal{F}_i(\xi,X)$ generates an infinite series when expanded in powers of ξ. In this respect our approach in fundamentally different from the adoption of a truncated polynomial representation for $\mathcal{F}_i(\xi,X)$ to generate nonparabolic free energy surfaces.[25,33]

In Eq. (11), λ_i is the solvent reorganization energy of ET in the ith state that is defined in the present article through the second cumulant of the reaction coordinate

$$\lambda_i=\beta\langle(\delta X)^2\rangle_i/2=-\frac{1}{2\beta}\left.\frac{\partial^2\mathcal{F}_i(\xi,0)}{\partial\xi^2}\right|_{\xi=0}. \quad (12)$$

In terms of the model parameters λ_i is given by the expression

$$\lambda_i=\frac{1}{2\kappa_i}(C_i/\alpha_i-\Delta C)^2, \quad (13)$$

where

$$\alpha_i=\frac{\kappa_i}{\Delta\kappa}, \quad (14)$$

$\Delta\kappa=\kappa_2-\kappa_1$, and $\Delta C=C_2-C_1$. The parameter α_i is of crucial importance for the present development. It defines the relative variation of the force constant of the classical collective mode of the solvent driving ET. The standard MH description of ET is recovered in the limit $\alpha_i\to\infty$ when the two force constants κ_i become equal.

An alternative definition of the reorganization energy in nonlinear systems used in the literature[34] is through half the Stokes shift. The two definitions coincide in the L-model, but differ in the Q-model. We prefer the definition of Eq. (12) because (*i*) the Stokes shift is observable only in the inverted region of ET and (*ii*) Eq. (12) involves average over only the equilibrium configuration of the solvent that is easier to treat by both computer simulations and equilibrium solvation theories. As two reorganization energies, for $i=1$ and $i=2$, are connected to each other (see later), the definition in Eq. (12) does not introduce additional theory parameters.

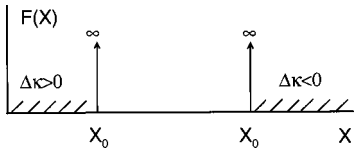

FIG. 1. One-sided fluctuation bands along the reaction coordinate X.

The parameter X_0 in Eq. (11) is defined through the equilibrium free energy gap $\Delta F_0=F_{02}-F_{01}$ and the reorganization energy as follows,

$$X_0=\Delta F_0-\lambda_1\frac{\alpha_1^2}{\alpha_2}=\Delta I-\frac{\Delta C^2}{2\Delta\kappa}, \quad (15)$$

where $\Delta I=I_2-I_1$. The coordinate X_0 sets up the boundary of the one-sided band of reaction coordinates (Fig. 1):

$$F_i(X)=\infty \quad \text{at } \Delta\kappa>0, \quad X<X_0, \quad (16)$$

and

$$F_i(X)=\infty \quad \text{at } \Delta\kappa<0, \quad X>X_0. \quad (17)$$

This property follows from the $|\xi|\to\infty$ asymptote $\mathcal{F}_i(\xi,X)\to i\xi\beta(X-X_0)$ and the fact that the generating function

$$\mathcal{G}_i(\xi,X)=\exp[\mathcal{F}_i(\xi,X)] \quad (18)$$

is analytic in the complex ξ-plane except the points of essential singularities at $i\alpha_i$. At $\Delta\kappa>0$ the essential singularities are in the upper half-plane. The integration contour closed in the lower half-plane at $X<X_0$ thus generates zero for the integral and, therefore, positive infinity for the ET free energy. Analogously, the integral is zero at $\Delta\kappa<0$ and $X>X_0$ (Fig. 1).

This important result indicates a fundamental distinction between the present Q-model and the MH theory.[10] The MH formulation, employing the L-model, leads to an unrestricted band of the energy gap fluctuations. This implies that any magnitude of the energy gap can be achieved with a nonzero, although even small, probability. On the contrary, the Q-model suggests a limited band for the energy gap fluctuations. The gap magnitudes achievable due to the nuclear fluctuations are limited by a low-energy boundary for $\Delta\kappa>0$ and by a high-energy boundary for $\Delta\kappa<0$. The probability of finding an energy gap fluctuation outside these boundaries is identically zero as there is no real solution of the equation $X=\Delta E$. This is the result of a bilinear dependence of the energy gap ΔE on the driving nuclear mode q, as is illustrated in Fig. 2.

The reorganization energies and parameters α_i in the two states are not independent and are connected by the following equations:

$$\alpha_1^3\lambda_1=\alpha_2^3\lambda_2 \quad (19)$$

and

$$\alpha_2=1+\alpha_1. \quad (20)$$

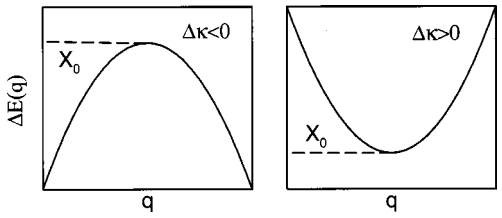

FIG. 2. The origin of the upper-energy ($\Delta\kappa<0$) and lower-energy ($\Delta\kappa>0$) fluctuation boundaries due to a bilinear dependence of ΔE on q.

These relations reduce the number of independent parameters of the model to three: ΔF_0, λ_1, and α_1. Compared to the two-parameter MH theory (λ and ΔF_0),[10] the present model introduces an additional flexibility in terms of the relative variation of the fluctuations force constant through α_1. The MH theory is recovered in the limit $\alpha_1\to\infty$. The permissible values of the parameter α_1 are constrained by the condition of the thermodynamic stability of the collective solvent mode in both states $\kappa_i>0$, resulting in two inequalities

$$\alpha_1>0 \quad \text{or} \quad \alpha_1<-1. \tag{21}$$

For X values inside the fluctuation band the contour integral includes the essential singularity at $i\alpha_i$ [see Eqs. (7) and (11)]. To evaluate the integral we will neglect the weak dependence of $\sqrt{g_i(\xi)}$ on ξ in the preexponent in Eq. (8) assuming $\sqrt{g_i(\xi)}=1$. (This approximation does not affect the good agreement between the numerical and analytical integration.) The integral is then calculated by expanding $\mathcal{G}_i(\xi,X)$ as follows:

$$\mathcal{G}_i(\xi,X)=e^{i\xi\beta(X-X_0)}\sum_{n=0}^{\infty}\frac{(-\beta\lambda_i\alpha_i^2)^n}{n!}\left(\frac{\xi}{\xi-i\alpha_i}\right)^n. \tag{22}$$

The residue calculus results in the relation

$$e^{-\beta F_i(X)+\beta F_{0i}}=\beta\lambda_i|\alpha_i|^3e^{-\beta|\alpha_i||X-X_0|}\times\sum_{n=0}^{\infty}\frac{(-\beta\lambda_i\alpha_i^2)^n}{(n+1)!}L_n^1(\beta|\alpha_i||X-X_0|), \tag{23}$$

where $L_n^m(x)$ is the Laguerre polynomial.[35] The sum can be converted to a closed-form solution[35]

$$e^{-\beta F_i(X)+\beta F_{0i}}=A_i\sqrt{\frac{\lambda_i|\alpha_i|^3}{|X-X_0|}}e^{-\beta(|\alpha_i||X-X_0|+\lambda_i\alpha_i^2)}I_1\times(2\beta\sqrt{|\alpha_i|^3\lambda_i|X-X_0|}), \tag{24}$$

where $I_1(x)$ is the first-order modified Bessel function. The normalization factor

$$A_i=(1-e^{-\beta\lambda_i\alpha_i^2})^{-1} \tag{25}$$

is included to ensure the identity

$$\beta\int_{-\infty}^{\infty}e^{-\beta F(X)+\beta F_{0i}}\,dX=1. \tag{26}$$

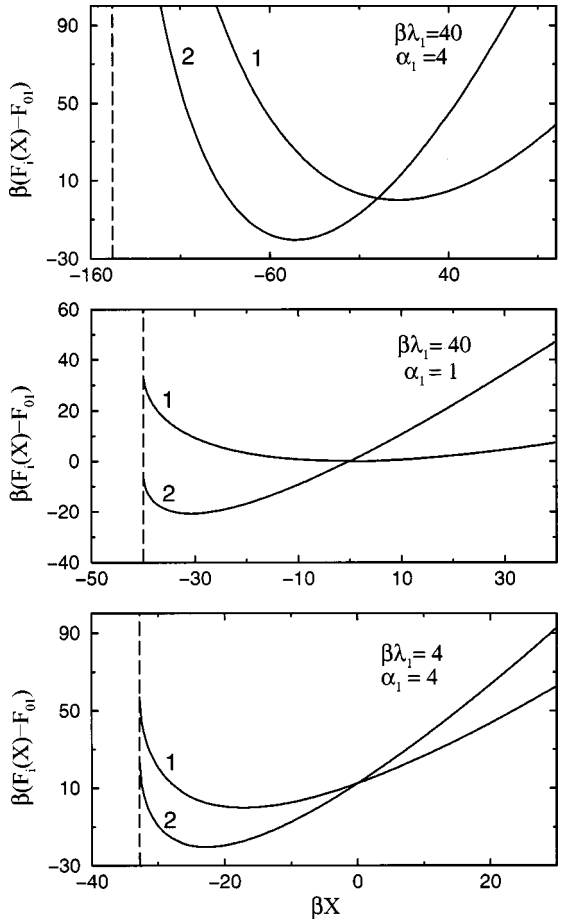

FIG. 3. $F_1(X)$ (1) and $F_2(X)$ (2) at various α_1 and $\beta\lambda_1$; $\Delta I=0$. The dashed line indicates the position of the fluctuation boundary X_0.

When X is not too close to X_0 and $2\beta\sqrt{|\alpha_i|^3\lambda_i|X-X_0|}\gg1$, a very simple equation for the ET free energies can be obtained by asymptotic expansion of the Bessel function[35] (the preexponential factor is neglected)

$$F_i(X)=F_{0i}+(\sqrt{|\alpha_i||X-X_0|}-|\alpha_i|\sqrt{\lambda_i})^2. \tag{27}$$

The above equation reduces to the standard high-temperature limit for the diabatic free energy surfaces of ET

$$F_i(X)=F_{0i}+\frac{(X-\Delta F_0\mp\lambda_i)^2}{4\lambda_i} \tag{28}$$

when $\alpha_i\gg1$ (the driving mode force constants κ_i in the two states are similar) and, additionally, $|X-\Delta F_0\mp\lambda_i|\ll|\alpha_i|\lambda_i$. Here, ''$-$'' and ''$+$'' correspond to $i=1$ and $i=2$, respectively. In the limit $|X-X_0|\gg\lambda_i|\alpha_i|$ the linear dependence holds:

$$F_i(X)=F_{0i}+|\alpha_i|\left|X-\Delta F_0+\lambda_1\frac{\alpha_1^2}{\alpha_2}\right|. \tag{29}$$

The free energy surfaces are asymmetric with the steeper branch on the side of the fluctuation boundary X_0. The other branch is less steep tending to a linear dependence at large X (Fig. 3). The minima of the initial and final free energy surfaces get closer to each other and to the band boundary with decreasing α_1 and λ_1. The crossing point then moves to the inverted ET region where the free energies are nearly linear

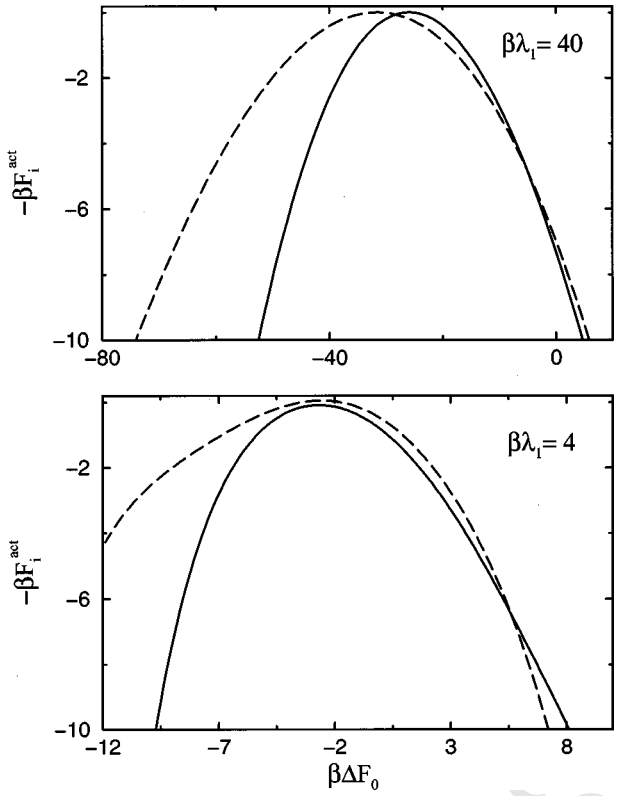

FIG. 4. Energy gap law for charge separation (dashed lines) and charge recombination (solid lines) at $\alpha_1=2.0$.

functions of the reaction coordinate. The linear energy gap law is then generated in the inverted ET region. Consequently, the whole energy gap dependence can be very asymmetric as is illustrated in Fig. 4.

The activation energy of ET follows from Eqs. (27)–(29) as

$$F_i^{\mathrm{act}}=F_i(0)-F_{0i}$$
$$=|\alpha_i|(\sqrt{|\Delta F_0-\lambda_1\alpha_1^2/\alpha_2|}-\sqrt{|\alpha_i|\lambda_i})^2. \quad (30)$$

Equation (30) produces the MH quadratic energy gap law at small $|\Delta F_0|\ll|\alpha_1\lambda_1|$ and yields a linear dependence of the activation energy on the equilibrium free energy gap at $|\Delta F_0-\lambda_1\alpha_1^2/\alpha_2|\gg|\alpha_i|\lambda_i$.

III. LINEAR RELATION: $F_2(X)=F_1(X)+X$

The transformation of the constrained trace in Eq. (5) is performed by representing the δ-function with the Fourier integral

$$\beta^{-1}\langle\delta(X-\Delta E)\rangle_2=\int_{-\infty}^{\infty}\frac{d\xi}{2\pi}\mathcal{G}_2(\xi,X)$$
$$=e^{\beta(\Delta F_0-X)}\int_{-i-\infty}^{-i+\infty}\frac{d\xi}{2\pi}\mathcal{G}_1(\xi,X). \quad (31)$$

One then obtains Eq. (5) provided the integrals over the segments $(-i-\infty,-i+\infty)$ and $(-\infty,+\infty)$ are equal. This is indeed true when $\mathcal{G}_1(\xi,X)$ is analytic in ξ inside the closed contour with the two segments as its boundaries. The function $\mathcal{G}_1(\xi,X)$ is not analytic if the essential singularity $\xi=i\alpha_i$ falls inside the integration contour. This happens when $-1\leqslant\alpha_1\leqslant 0$. This, according to Eq. (21), implies that the driving nuclear mode loses its thermodynamic stability in the initial or final ET state. The validity of the linear relation between the diabatic free energy surfaces [Eq. (4)] is thus equivalent to thermodynamic stability of the nuclear mode driving ET.

It is easy to see that linear relation (4) does hold for the Q-model. Since the product $|\alpha_i^3\lambda_i|$ is an invariant of the electronic state [Eq. (19)], the Bessel function term in Eq. (24) is an invariant, too. Therefore, one obtains from Eq. (24)

$$F_2(X)-F_1(X)=\Delta F_0+(|\alpha_2|-|\alpha_1|)|X-X_0|+\lambda_2\alpha_2^2$$
$$-\lambda_1\alpha_1^2. \quad (32)$$

Since $(|\alpha_2|-|\alpha_1|)|X-X_0|\equiv(X-X_0)$, Eq. (4) follows from Eq. (32) and the definition of the fluctuation boundary X_0 in Eq. (15).

IV. MODEL PARAMETERS

The success of the MH theory[10] in application to thermal and optical CT transitions can, to a large degree, be attributed to the fact that the two parameters entering the theory, the reorganization energy and the equilibrium energy gap, can be connected to spectroscopic observables. The first spectral moments

$$\hbar\omega_i=\langle X\rangle_i=\int_{-\infty}^{\infty}Xe^{-\beta F_i(X)}\,dX\Big/\int_{-\infty}^{\infty}e^{-\beta F_i(X)}\,dX \quad (33)$$

fully define λ and ΔF_0 through the mean energy $\hbar\omega_{\mathrm{m}}=\hbar(\omega_1+\omega_2)/2$ and the Stokes shift $\hbar\Delta\omega_{\mathrm{st}}=\hbar(\omega_1-\omega_2)/2$ as

$$\hbar\omega_{\mathrm{m}}=\Delta F_0 \quad (34)$$

and

$$\hbar\Delta\omega_{\mathrm{st}}=2\lambda. \quad (35)$$

The Q-model involves an additional parameter α_1 that can be determined by invoking the second spectral moments in addition to the first moments. The solvent reorganization energy has been defined above through the second cumulant of the reaction coordinate X that corresponds to the second spectral cumulant

$$\lambda_i=\beta\langle(\delta X)^2\rangle_i/2=\beta\hbar^2\langle\delta\omega^2\rangle_i/2 \quad (36)$$

representing the optical bandwidth.

The first spectral moment is given in the present model by the relation

$$\langle X\rangle_i=-(i\beta)^{-1}\frac{\partial\mathcal{F}_i(\xi,0)}{\partial\xi}\bigg|_{\xi=0}=X_0+\alpha_i\lambda_i. \quad (37)$$

From Eqs. (20) and (37) one obtains the parameter α_1:

$$\alpha_1=-\Delta\lambda^{-1}(\hbar\Delta\omega_{\mathrm{st}}+\lambda_2),\quad \Delta\lambda=\lambda_2-\lambda_1. \quad (38)$$

Similarly, the equilibrium energy gap is

$$\Delta F_0 = \hbar\omega_m - \frac{\lambda_1}{2}\frac{\alpha_1}{\alpha_2^2}, \tag{39}$$

which is equivalent to[36]

$$\Delta F_0 = \hbar\omega_m + \frac{\lambda_1\Delta\lambda}{2}\frac{\hbar\Delta\omega_{st}+\lambda_2}{(\hbar\Delta\omega_{st}+\lambda_1)^2}. \tag{40}$$

The Stokes shift and two second spectral moments fully define the parameters of the model. In addition, they should satisfy Eqs. (19) and (20). The latter feature is important for mapping the model onto condensed-phase simulations of ET that we consider next.

V. PHYSICAL REALIZATIONS OF THE MODEL

The MH two-parameter model provides a mathematical realization of the concept of linear coupling of solute electronic states to a harmonic solvent bath (L-model). The three-parameter Q-model yields more flexibility by including an additional parameter α_1 quantifying the extent of the force constant variation of the nuclear mode driving ET. The two models are equivalent in the limit $\alpha_1 \to \infty$. The MH model has been successfully mapped onto several real ET systems[37(a)] and, more generally, on condensed-phase reactions involving redistribution of the charge density.[37(b)] However, limitations imposed by the condition $\kappa_1 = \kappa_2$ inherent in the L-model do not allow its application to more complex physical phenomena characterized by nonparabolic free energy surfaces. Below, we discuss some physical realizations of the mathematical Q-model developed above.

A. Nonlinear solvation

The CT spectra and kinetic data often do not provide direct information about the ET free energy surfaces. In the absence of reliable experimental data, computer simulations[5,6] and liquid-theory calculations[22] have been undertaken for a number of model systems. In this connection, the influence of nonlinear solvation on the ET energetics has become an issue of close scrutiny.[5,24] The problem is usually addressed either through direct generation of $F_i(X)$ by umbrella-sampling techniques[5,6] or by computing a few cumulants at the initial and final equilibrium states.[22(b)] In both cases, the absence of a closed-form, analytical solution involving the nonlinear coupling makes it difficult to represent the numerical data by a formula conforming with the linear relation, Eq. (4). This drawback also makes it impossible to extrapolate the numerical results outside the simulation range and to generate analytical continuation to the complex plane of solute multipoles.[38] These restrictions impede application of the simulation results to generating optical spectra and the energy gap law.

As is shown in the previous section, only two equilibrium moments for each ET state are sufficient to determine the model parameters. This presents, of course, a considerable advantage as only initial and final equilibrium configurations of the ET system can be sampled generating the global, nonequilibrium free energy surfaces. This goal is, however, achievable only if the Q-model can be mapped onto a real or simulated condensed-phase ET system. A crucial test is provided from Eq. (19), which indicates that the parameter

$$\gamma = \frac{\alpha_1^3\lambda_1}{\alpha_2^3\lambda_2} \tag{41}$$

calculated from the simulated reorganization energies and minima positions [Eqs. (36) and (38)] should be equal to unity. In fact, many simulations showing nonlinear solvation effects can be mapped on the Q-model. Table I lists the parameters α_1 and γ calculated from the simulation results reported in the literature. The condition $\gamma = 1$ holds very accurately.

Our own simulations (in the Appendix) also show that the condition of the model consistency $\gamma = 1$ is fulfilled very well for dipolar solutes of various magnitudes of the dipole moment m_{0i} in a solvent of hard sphere (HS) permanent dipoles forming a liquid or an *fcc* lattice (Table II). The simulations were performed in different phase states of the solvent for a given charge distribution of the solute in order to address the question as to which solvation environment results in stronger nonlinear solvation. In order to quantify the nonlinear effect, we plotted in Fig. 5 the parameter $1/\alpha_1$ and the ratio

$$\chi_i = \frac{2\lambda_i}{|\langle X\rangle_1 - \langle X\rangle_2|} \tag{42}$$

against the variation of the solute dipole with ET. For linear solvation, $1/\alpha_1 = 0$ and $\chi_i = 1$. Both parameters indicate that the dipolar lattice produces a much stronger nonlinear solvation effect compared to the fluid solvent with equal molecular properties. The variation of the force constant κ_i is up to 20% in the dipolar lattice. The inclusion of the isotropic molecular polarizability of the solvent (up triangles in the upper panel of Fig. 5) considerably diminishes the nonlinear effect (cf. Tables II and III), in contrast to the opposite trend reported previously.[7(b)] Note that the condition $\gamma = 1$ still holds for the polarizable solute and solvent (Table III[39]).

A comparison of the results for the dipolar fluid and dipolar lattice in Table II indicates a considerable difference in solvation for these two media. For instance, the reorganization energy of the high-dipole state with $\Delta m_0/m = 8.0$ ($\Delta m_0 = m_{02} - m_{01}$) is about 50% higher in the dipolar fluid compared to the dipolar lattice for equal polarities of the constituent molecules. The shift $-\beta\langle X\rangle_2$ is about 34% higher in the fluid solvent. This is an indication of a stronger solvating power of the fluid solvent due to the ability of the solvent molecules to adjust their packing around a solute. The rearrangement of the coordinates of the solvent molecules also reduces the saturation of the orientational response, diminishing the nonlinear solvation effect. This compensation does not exist in a lattice solvent resulting in a considerably stronger nonlinear effect, in agreement with analogous observations reported previously.[25]

The solvation parameters listed in Table II do not describe the physical phenomenon of a random impurity solvation in an *fcc* lattice. The solvation shift $\langle X\rangle_i$ and the reorganization energy, measured from simulations, both depend

TABLE II. Reorganization parameters for a dipolar transition $m_{01} \rightarrow m_{02}$ with $m_{01}/m = 2.0$ and $\Delta m_0 = m_{02} - m_{01}$. The solute is a dipolar hard sphere with the radius $R_0/\sigma = 0.9$. The solvent is composed of dipolar hard spheres (DHS) of diameter σ and a dipole moment m in the liquid and *fcc* solid phases; $\beta m^2/\sigma^3 = 1.0$.

$\Delta m_0/m$	$-\beta\langle X\rangle_1$	$\beta\lambda_1$	$-\beta\langle X\rangle_2$	$\beta\lambda_2$	$\beta^3\langle(\delta X)^3\rangle_2/6$	$\beta^3\langle(\delta X)^3\rangle_2/6$[a]	α_1	γ[b]
				DHS liquid[c]				
4	4.70	4.56	14.15	4.29	(0.17)[d]	0.08	51	1.003
5	5.88	7.25	20.09	6.54	(0.41)[d]	0.17	38	1.005
6	7.05	10.26	27.45	9.07	(0.49)[d]	0.31	29	1.001
7	8.23	13.97	35.60	12.00	(0.59)[d]	0.59	20	1.005
8	9.40	18.24	44.59	15.17	(1.03)[d]	0.98	14	1.009
				DHS lattice[e]				
4	4.20	3.96	10.86	2.95	(0.22)	0.28	9.5	0.995
5	5.25	6.19	15.77	4.39	(0.52)	0.47	8.3	1.002
6	6.30	8.91	20.93	5.89	(0.42)	0.76	6.8	1.002
7	7.35	12.13	26.76	7.66	(0.65)	1.09	6.1	1.001
8	8.40	15.84	33.13	9.65	(0.84)	1.47	5.6	0.999

[a]Calculated according to Eq. (43).
[b]From Eq. (41).
[c]$N = 864$ solvent molecules in the simulation box.
[d]From computer simulations with $N = 864$ solvent molecules in the simulation box. The values are given in parentheses as they change substantially when switching from $N = 500$ to $N = 864$.
[e]$N = 494$.

on the coordinate of the point at which solute is inserted into the lattice. For instance, simulations with $N = 851$ lattice molecules give $\beta\langle X\rangle_2 = 19.0$ and $\beta\lambda_2 = 6.4$ at $\Delta m_0/m = 8.0$. This is considerably different from $\beta\langle X\rangle_2 = 33.13$ and $\beta\lambda_2 = 9.7$ at $N = 494$, not because of the limited size of the simulation box which does not allow the thermodynamic limit, but due to the fact that the solute inserted in the center of the simulation box generates different local environments depending on N when the overlapping lattice molecules are removed. Lattice simulations, therefore, cannot be used to model disordered impurity solvation in solids, as well as they cannot be used to represent solvation in fluid solvents.

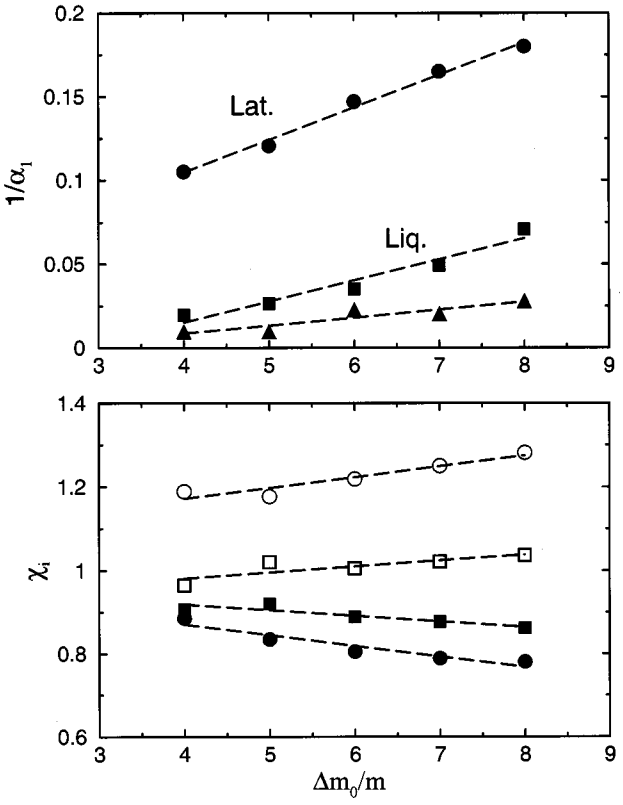

FIG. 5. Upper panel: $1/\alpha_1$ vs $\Delta m_0/m$. Lower panel: the parameter χ_i [Eq. (42)] for $i = 1$ (open points) and $i = 2$ (filled points) vs $\Delta m_0/m$. $1/\alpha_1 = 0$ and $\chi_i = 1$ for linear solvation. Circles indicate the lattice DHS solvent; squares correspond to a liquid DHS solvent. The up triangles in the upper panel indicate nonpolarizable solutes in a polarizable DHS liquid; $\beta m^2/\sigma^3 = 1$, $\alpha/\sigma^3 = 0.05$.

The present simulations (Tables II and III) and those reported in the literature (Table I) both indicate that nonlinear effects of solvation saturation obey the consistency condition $\gamma = 1$ of the Q-model. This suggests that nonlinear solvation effects can be successfully mapped onto the model. The simulations do not, however, give a definite answer as to whether the Q-model is capable of reproducing the third cumulant[40]

$$\beta^3\langle(\delta X)^3\rangle_i = -i\left.\frac{\partial^3 \mathcal{F}_i(\xi,0)}{\partial \xi^3}\right|_{\xi=0} = \frac{6\beta\lambda_i}{\alpha_i}. \tag{43}$$

The third cumulants listed in Table II do not reach the thermodynamic limit as they substantially depend on the number of particles in the simulation box.[41] They are, however, uniformly small compared to the second cumulants and the analytical free energies $F_i(X)$ [Eq. (24)] are very close to those generated by computer simulations (Fig. 6). In order to demonstrate this, Fig. 6 shows the results obtained for solvation of dipolar solutes by the dipolar lattice where nonlinear effects assume the greatest importance.

Two routes to calculate the free energy surfaces from simulations have been accepted. In the first approach, a polynomial fit of the simulated equilibrium solute–solvent energies $u_{0s}^{(i)}(m_0) = \langle U_{0s}\rangle_i$ (U_{0s} is the solute–solvent interaction potential energy) versus the solute dipole m_0 was used to determine the solvation chemical potential[27]

$$\mu_{pi}(m_0) = \int_0^{m_0} \frac{dm}{m} u_{0s}^{(i)}(m) \tag{44}$$

TABLE III. Reorganization parameters for a dipolar transition $m_{01}\rightarrow m_{02}$ with $m_{01}/m=2.0$ and $\Delta m_0=m_{02}-m_{01}$. The solute is a nonpolarizable ($\alpha_0^*=0$) or a polarizable ($\alpha_0^*=\alpha_0/\sigma_0^3=0.05$) dipolar hard sphere with the radius $R_0/\sigma=0.9, 2R_0=\sigma_0$. The solvent is composed of dipolar polarizable hard spheres of diameter σ, polarizability $\alpha^*=\alpha/\sigma^3=0.05$, and the dipole moment $\beta m^2/\sigma^3=1.0$.

$\Delta m_0/m$	$-\beta\langle X\rangle_1$	$\beta\lambda_1$	$-\beta\langle X\rangle_2$	$\beta\lambda_2$	α_1	γ
			Non polarizable solute[a]			
4	5.4	4.0	16.0	3.9	104	1.006
5	6.7	6.3	23.4	6.1	71	1.009
6	8.0	9.1	32.2	8.4	44	1.018
7	9.4	12.4	42.0	11.5	51	1.014
8	10.7	16.2	53.3	14.6	36	1.021
			Polarizable solute[a]			
4	5.6	4.2	17.8	4.1	154	1.006
5	7.0	6.5	24.1	6.2	76	1.009
6	8.4	9.4	32.9	9.0	80	1.008
7	9.8	12.8	42.8	11.9	49	1.013
8	11.2	16.7	54.3	15.4	48	1.014

[a]With $N=256$ solvent molecules in the simulation box.

and then the ET free energies[25,38]

$$F_i(X)-F_{0i}=-\beta^{-1}\ln\left[\int_{-\infty}^{\infty}\frac{ds}{2\pi}\exp(is\beta(X-\Delta I)-\beta\mu_{pi}(m_{0i}+is\Delta m_0)+\beta\mu_{pi}(m_{0i}))\right]. \tag{45}$$

The second route employs the truncated cumulant expansion with the first three cumulants determined from computer simulations such that

$$F_i(X)-F_{0i}=-\beta^{-1}\ln\left[\int_{-\infty}^{\infty}\frac{ds}{2\pi}\exp\left(is\beta(\Delta I+u_{0s}^{(i)}-X)+\sum_{n=2,3}\frac{(is)^n}{n!}K_i^{(n)}\right)\right], \tag{46}$$

$$K_i^{(n)}=\beta^n\langle(\delta\Delta U_{0s})^n\rangle_i, \quad n\geqslant 2. \tag{47}$$

Figure 6 shows that the analytical free energy surfaces of the Q-model coincide on the scale of the plot with the free energies from simulations. The left-most branch of the surface obtained from Eqs. (44) and (45) (short-dashed line) falls outside the range of simulated equilibrium energies and illustrates the danger of extrapolating the local simulation results to produce global free energy surfaces. It should be noted that since the two free energy surfaces are connected by the linear relation [Eq. (4)], a comparison of the simulated and analytically calculated surfaces in the initial state ($i=1$) is sufficient to draw a conclusion as to their agreement.

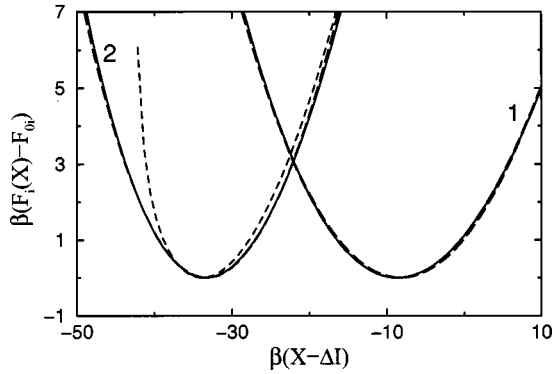

FIG. 6. $F_1(X)$ (1) and $F_2(X)$ (2) from the analytical Q-model (solid lines), from the equilibrium chemical potential [Eqs. (45) and (44), short-dashed lines], and from the truncated cumulant expansion [Eqs. (46) and (47), long-dashed lines]. The transition $m_{01}\rightarrow m_{02}$ with $m_{01}/m=2$ and $m_{02}/m=10$ in the dipolar lattice with $\beta m^2/\sigma^3=1.0$ is considered; $R_0/\sigma=0.9$.

B. Polarizable ET complexes

The instantaneous energy of a dipolar polarizable solute with the isotropic polarizability α_{0i} in a condensed solvent[3] depends on the nuclear configuration of the solvent through the reaction field of the nuclear polarization $\mathbf{R}_p$ such that[42]

$$E_i=I_i-\tilde{\mathbf{m}}_{0i}\cdot\mathbf{R}_p-(\tilde{\alpha}_{0i}/2)\mathbf{R}_p^2+(4a_p)^{-1}\mathbf{R}_p^2. \tag{48}$$

The effective solute dipole, $\tilde{m}_{0i}=f_{ei}m_{0i}$, and the effective polarizability, $\tilde{\alpha}_{0i}=f_{ei}\alpha_{0i}$, in the ith state are enhanced compared to their vacuum values m_{0i} and α_{0i} by the factor

$$f_{ei}=[1-2a_e\alpha_{0i}]^{-1}. \tag{49}$$

The enhancement of the dipole moments and the polarizabilities is the result of the self-consistent effect of the field of the electronic polarization of the solvent. The response functions a_e and a_p in Eqs. (48) and (49) generate the solvation chemical potential due to the electronic polarization, $\mu_{ei}=-a_ef_{ei}m_{0i}^2$, and the solvation chemical potential by the nuclear solvent modes, $\mu_{pi}=-(af_i-a_ef_{ei})m_{0i}^2$. Here, $a=a_p+a_e$ and

$$f_i=[1-2a\alpha_{0i}]^{-1}. \tag{50}$$

A comparison of Eqs. (6) and (48) reveals that the Q-model is equivalent to the problem of ET in linearly polarizable CT complexes. The parameters of two models are connected by the relations

$$\kappa_i=(2a_p)^{-1}-\tilde{\alpha}_{0i} \tag{51}$$

and

$$C_i = \tilde{m}_{0i}. \tag{52}$$

Further, one obtains

$$\Delta\kappa = -\Delta\tilde{\alpha}, \quad \Delta\tilde{\alpha} = \tilde{\alpha}_{02} - \tilde{\alpha}_{01}. \tag{53}$$

Therefore, the common situation of the solute polarizability increasing with excitation[3] corresponds to $\Delta\kappa < 0$. The sign of the force constant change is then opposite to the effect of nonlinear solvation yielding $\Delta\kappa > 0$.[43]

From the connection between the solute properties and model parameters [Eqs. (51) and (52)] and the reorganization energy in the Q-model [Eq. (13)] one obtains the reorganization energy of ET in a solute with both the dipole moment and the polarizability changing with the transition

$$\lambda_1 = (a_p f_1 / f_{e1})(\Delta\tilde{\mathbf{m}} + 2a_p f_1 \Delta\tilde{\alpha}\mathbf{m}_{01})^2. \tag{54}$$

Also, the parameter α_1 becomes

$$\alpha_1 = -\frac{f_{e1}}{2a_p f_1 \Delta\tilde{a}} \tag{55}$$

and the equilibrium energy gap takes the form

$$\Delta F_0 = \Delta I - a_p f_{e2} f_2 m_{02}^2 + a_p f_{e1} f_1 m_{01}^2 \tag{56}$$

(the solvation free energy by the electronic solvent polarization is included in ΔI). Equation (55) indicates that the physical reason for a finite value of α_1 for polarizable ET complexes is solvation of the induced solute dipole by the nuclear field of the solvent. The strength of this field is defined by the parameter a_p increasing with solvent polarity. Accordingly, the nonlinear effect of the polarizability variation increases with solvent polarity.

The connection of the model parameters to spectroscopic moments leads to the relation for the polarizability change

$$\Delta\tilde{\alpha} = \frac{1}{2\lambda_1}\frac{\Delta\lambda}{\hbar\Delta\omega_{\mathrm{st}} + \lambda_2}\left(\tilde{\mathbf{m}}_{02} - \tilde{\mathbf{m}}_{01}\frac{\hbar\Delta\omega_{\mathrm{st}} + \lambda_1}{\hbar\Delta\omega_{\mathrm{st}} + \lambda_2}\right)^2. \tag{57}$$

In many practical cases the factors f_{ei} are very close to unity and can be omitted. The parameters $\tilde{\alpha}_{0i}$ and $\tilde{\mathbf{m}}_{0i}$ are then equal to their vacuum values α_{0i} and $\mathbf{m}_{0i}$ and Eq. (57) gives the polarizability change in terms of spectroscopic moments and vacuum solute dipoles. Experimental measurement and theoretical calculation of $\Delta\alpha_0 = \alpha_{02} - \alpha_{01}$ are still challenging. Perhaps the most accurate way to measure $\Delta\alpha_0$ presently available is that by Stark spectroscopy,[44,45] which also gives Δm_0. Equation (57) can therefore be used as an independent source of $\Delta\alpha_0$, provided all other parameters are available, or as a consistency test for the bandshape analysis.

C. Configurational flexibility of CT complexes

Consider a CT complex with the vacuum field $\mathbf{D}_i(Q)$ in a polar solvent. The field creates a polarization of the solvent, and the electronic energy in the ith state can be expressed as

$$I_i - \mathbf{P}_p \cdot \mathbf{D}_i(Q), \tag{58}$$

where the scalar product indicates integration over the solvent volume V

$$\mathbf{P}_p \cdot \mathbf{D}_i = \int_V \mathbf{P}_p(\mathbf{r}) \cdot \mathbf{D}_i(\mathbf{r})\, d\mathbf{r}. \tag{59}$$

In Eqs. (58), $\mathbf{P}_p$ is the nuclear solvent polarization. The solute field in the above equation depends on a classical intramolecular mode Q changing from the equilibrium value Q_{01} to the equilibrium value Q_{02} with the transition. We assume that $\mathbf{D}_i(Q)$ can be expanded in a series in $(Q - Q_{0i})$ and truncate the expansion at the linear order term

$$\mathbf{D}_i(Q) = \mathbf{D}_i(Q_{0i}) + \mathbf{D}'_{Qi}(Q - Q_{0i}) \quad \mathbf{D}'_{Qi} = \left.\frac{\partial \mathbf{D}(Q)}{\partial Q}\right|_{Q_{0i}}. \tag{60}$$

For harmonic classical modes $\mathbf{P}_p$ and Q one obtains for the instantaneous energies

$$E_i = I_i - \mathbf{P}_p \cdot \tilde{\mathbf{D}}_{0i} - Q\mathbf{D}'_{Qi} \cdot \mathbf{P}_p + \frac{\kappa_Q}{2}Q^2 + \frac{\kappa_P}{2}\mathbf{P}_p \cdot \mathbf{P}_p, \tag{61}$$

where κ_Q and κ_P are the force constants of the corresponding nuclear modes and

$$\tilde{\mathbf{D}}_{0i} = \mathbf{D}_i(Q_{0i}) - Q_{0i}\mathbf{D}'_{Qi}. \tag{62}$$

In the dielectric continuum approximation for the microscopic polarization $\mathbf{P}_p$ the force constant is $\kappa_P = 4\pi/c_0$, where c_0 is the Pekar factor.

For two nuclear, classical modes the ET free energy surfaces are given by the expression

$$e^{-\beta F_i(X) + \beta F_{0i}} = \beta^{-1}\langle \delta(X - \Delta E)\rangle_{i,QP}, \tag{63}$$

where the subscript ''QP'' denotes the equilibrium average over the Q and $\mathbf{P}$ modes. Both are quadratic and the average is straightforward. Representing the δ-function by the Fourier integral as in Eq. (7) and performing the average over Q one gets the terms quadratic and linear in the integration variable ξ. The first term is proportional to $(\Delta\mathbf{D}'_Q \cdot \mathbf{P}_p)^2$ and the second is proportional to $(\Delta\mathbf{D}'_Q \cdot \mathbf{P}_p)(\mathbf{D}'_{Qi} \cdot \mathbf{P}_p)$ where

$$\Delta\mathbf{D}'_Q = \mathbf{D}'_{Q2} - \mathbf{D}'_{Q1}. \tag{64}$$

The variation $\Delta\mathbf{D}'_Q$ is nonvanishing only due to the nonlinear terms in the dependence of $\mathbf{D}_i(Q)$ on Q. The quadratic in $\Delta\mathbf{D}'_Q$ terms can thus be neglected compared to the terms linear in $\Delta\mathbf{D}'_Q$. In this approximation, by representing the field $\mathbf{D}'_{Qi}$ as $\mathbf{D}'_{Qi} = \overline{\mathbf{D}}'_Q \pm \Delta\mathbf{D}'_Q$, $\overline{\mathbf{D}}' = (\mathbf{D}'_{Q2} + \mathbf{D}'_{Q1})/2$, we drop the terms quadratic in $\Delta\mathbf{D}'_Q$. The free energy surfaces then become

$$e^{-\beta F_i(X) + \beta F_{0i}} = \beta^{-1}\langle \delta(X - \Delta\tilde{E}_i)\rangle_{i,P}, \tag{65}$$

with

$$\Delta\tilde{E}_i = \Delta I - \Delta\tilde{\mathbf{D}} \cdot \mathbf{P}_p - \frac{1}{\kappa_Q}(\Delta\mathbf{D}'_Q \cdot \mathbf{P}_p)(\overline{\mathbf{D}}'_Q \cdot \mathbf{P}_p) \tag{66}$$

and $\Delta\tilde{\mathbf{D}} = \tilde{\mathbf{D}}_{02} - \tilde{\mathbf{D}}_{01}$.

The equation for $\Delta\tilde{E}_i$ is formally equivalent to that for a polarizable CT solute with an anisotropic polarizability. In order to bring the system in accord with the Q-model, the last term in Eq. (66) is averaged over the orientations of the polarization field $\mathbf{P}_p$. The effective instantaneous energies

TABLE IV. Main features of the two-parameter L-model (MH) and the three-parameter Q-model.

	L-model	Q-model
Parameters	ΔF_0, λ	ΔF_0, λ_1, α_1
Reaction coordinate	$-\infty<X<\infty$	$X>X_0$ at $\alpha_1>0$ $X<X_0$ at $\alpha_1<0$
Spectral moments	$\Delta F_0=\hbar\omega_m$ $\lambda=\hbar\Delta\omega_{st}/2$	$\Delta F_0=\hbar\omega_m-\lambda_1\alpha_1/2(1+\alpha_1)^2$ $\lambda_1=\beta\hbar^2\langle(\delta\omega)^2\rangle_1/2$ $\alpha_1=(\hbar\Delta\omega_{st}+\lambda_2)/(\lambda_1-\lambda_2)$
Energy gap law		
$\Delta F_0+\lambda_1\ll\lambda_1$	$F_1^{act}\propto(\Delta F_0+\lambda)^2$	$F_1^{act}\propto(\Delta F_0+\lambda_1)^2$
$\lvert\Delta F_0\rvert\gg\lambda_1$	$F_1^{act}\propto\Delta F_0^2$	$F_1^{act}\propto\lvert\Delta F_0\rvert$

$$\tilde{E}_i=I_i-\tilde{\mathbf{D}}_{0i}\cdot\mathbf{P}_p-\frac{1}{3\kappa_Q}(\mathbf{D}'_{Qi}\cdot\tilde{\mathbf{D}}'_Q)(\mathbf{P}_p\cdot\mathbf{P}_p) \tag{67}$$

are then isomorphic to the Q-model [Eq. (6)] with

$$\mathbf{C}_i=\tilde{\mathbf{D}}_{0i}, \tag{68}$$

$$\kappa_i=\kappa_P-\frac{2}{3\kappa_Q}(\mathbf{D}'_{Qi}\cdot\tilde{\mathbf{D}}'_Q), \tag{69}$$

and

$$\Delta\kappa=-\frac{2}{3\kappa_Q}(\Delta\mathbf{D}'_Q\cdot\tilde{\mathbf{D}}'_Q). \tag{70}$$

Equations (68) and (69) directly lead to the reorganization parameters and the ET free energy surfaces in the framework of the Q-model. As these parameters are also connected to spectroscopic observables, one thus gains a tool for studying optical and thermal ET in configurationally flexible molecules. The effect of the intramolecular mode is reflected in the modulation of the effective force constant of the Gaussian solvent fluctuations. This effect increases with a softening of the intramolecular mode. Such soft conformational modes are encountered for protein ET where large amplitude fluctuations of the protein matrix have the potential of considerable variation of the donor–acceptor distance. Furthermore, twisted ET is accompanied by a variation of the dihedral angle ϕ between the donor and acceptor groups.[46] In the latter case, the chromophore dipole moment $\mathbf{m}_{0i}$ depends on the dihedral angle and $\mathbf{D}'_{Qi}\propto\mathbf{m}'_{\phi i}$. If all the dipoles are collinear, one obtains

$$\Delta\kappa=-\frac{4}{3\kappa_\phi\kappa_P}\frac{\Delta m'_\phi\tilde{m}'_\phi}{\Delta m^2}\lambda_s, \tag{71}$$

where $\lambda_s=(\kappa_P/2)\Delta\mathbf{D}_0\cdot\Delta\mathbf{D}_0$, and $\Delta\mathbf{D}_0=\mathbf{D}(\phi_{02})-\mathbf{D}(\phi_{01})$ is the MH definition for the solvent reorganization energy. The present mapping of the CT complexes with flexible configurations onto the Q-model contains several approximations that need testing. In particular, the exact average in Eq. (63) goes beyond the Q-model, resulting in stronger nonlinear effects than those reflected by the Q-model. A more detailed study of this problem will be presented elsewhere.[47]

VI. CONCLUSIONS

This article presents a three-parameter model for the free energy surfaces of ET in condensed phases. It extends the two-parameter (λ and ΔF_0) MH model by introducing the third parameter α_1 reflecting the variation of the force constant of the classical solvent mode driving ET. The model is equivalent to that of a solute bilinearly coupled to a harmonic solvent mode. The exact solution obtained here leads to nonparabolic free energy surfaces of ET that obey the fundamental linear relation given by Eq. (4). Its validity is equivalent to the condition of thermodynamic stability of the driving solvent mode. Compared to the MH model, the present development predicts a more diverse pattern of possible system regimes including (*i*) an existence of a one-sided band restricting the range of permissible reaction coordinates, (*ii*) singular free energies outside the fluctuation band, and (*iii*) a linear energy gap law at large activation barriers. The model parameters are fully defined by the first two equilibrium cumulants of the ET reaction coordinate. This allows construction of global, nonparabolic free energy surfaces from spectroscopic measurements and/or equilibrium computer simulations. The main features of the present and MH models are compared in Table IV.

The mathematical model (Q-model) developed here is capable of reproducing several physical situations which conflict with the assumptions of the MH model. In this regard, we have shown that nonlinear solvation by solid and liquid solvents can be described by the Q-model. The condition for the model consistency holds both for our own simulations and those reported in the literature. The Q-model is shown to be isomorphic to the problems of electronic transitions in linearly polarizable CT complexes and CT complexes with configurational flexibility.

Perhaps more important than particular physical realizations of the model is the fundamental physical picture arising from the analysis of the solution. The free energy surfaces are discontinuous at the boundary of the fluctuation band tending to positive infinity. Of course, higher order expansion terms in the solute–solvent coupling may eliminate the singularity replacing it by a steep ascent or a finite jump. The existence of such a strongly nonlinear behavior may be useful for applications. Such nonlinearities of ET energetics may, for example, be responsible for a very efficient stabilization of charge-separated states in natural photosynthetic centers[11(c)] or be utilized in the molecular design of new materials for energy storage.[48]

ACKNOWLEDGMENTS

This research was supported by the Basic Energy Sciences Branch of the Department of Energy through Grant No. DE-FG03-99ER14963.

APPENDIX A: COMPUTER SIMULATIONS OF NONLINEAR SOLVATION

The Monte Carlo (MC) simulations were carried out for a dipolar solute in liquid and solid solvents composed of dipolar hard spheres. Solvation of polarizable and nonpolarizable dipolar solutes was also simulated in the liquid of dipolar/polarizable hard spheres with the isotropic dipolar polarizability $\alpha^* = \alpha/\sigma^3 = 0.05$; σ is the hard sphere diameter of the solvent molecules. The initial system configuration was generated by inserting a solute of of a small size into a cubic simulation cell with the solvent molecules occupying the sites of an *fcc* cubic lattice. The solute size was then gradually increased in the course of standard MC runs. The overlapping configurations were avoided by translations of the solvent molecules in the liquid solvent; the solvent molecules of the *fcc* lattice overlapping with the solute were removed from the simulation box. Stochastic translations and rotations of the solvent molecules were generated for the liquid phase and only rotations were allowed for the *fcc* lattice. Simulations of the polarizable systems were performed by self-consistent adjusting of the solvent- and/or solute-induced dipole to the electric field of the medium following each simulation step consisting of a translation and rotation of a molecule.[49] Molecules inside three solvation shells surrounding the moved particle were included to calculate the field. This reduces the CPU time and generates the results indistinguishable from those with all molecules in the simulation box used to calculate the field. Periodic boundary conditions with the minimum image convention along with the reaction-field correction for the dipole–dipole interactions (reaction field dielectric constant equal to 1000) were employed.[50]

The nonpolarizable systems were simulated with $N = 500$ and 864 solvent molecules in the simulation box for the liquid solvent and $N = 494$ and 851 solvent molecules for the *fcc* lattice. Solvation in the polarizable liquid solvent was simulated with $N = 256$ and 500 solvent molecules. For both polarizable and nonpolarizable liquid solvents, no dependence on N for the first two measured moments of the solute–solvent interaction potential energy has been observed. The third moment drops substantially when switching from $N = 256$ to $N = 500$ in the polarizable liquid and from $N = 500$ and 864 in the nonpolarizable liquid solvent. About 72 hours of CPU time are necessary for each 100 000 configurations of a polarizable liquid of $N = 500$ molecules on a Pentium-III 550 MHz processor. When the solute is inserted in the center of the *fcc* lattice, all simulation results considerably depend on N as different local solvent environments are generated by removing the overlapping solvent molecules.

[1] J. N. Gehlen, D. Chandler, H. J. Kim, and J. T. Hynes, J. Phys. Chem. **96**, 5088 (1992).
[2] D. V. Matyushov and B. M. Ladanyi, J. Chem. Phys. **108**, 6362 (1998).
[3] D. V. Matyushov and G. A. Voth, J. Phys. Chem. A **103**, 10981 (1999).
[4] M. Lax, J. Chem. Phys. **20**, 1752 (1955).
[5] (a) A. Warshel, J. Phys. Chem. **86**, 2218 (1982). (b) J.-K. Hwang and A. Warshel and J. Am. Chem. Soc. **109**, 715 (1987). (c) G. King and A. Warshel, J. Chem. Phys. **93**, 8682 (1990).
[6] R. A. Kuharski, J. S. Bader, D. Chandler, M. Sprik, M. L. Klein, and R. W. Impey, J. Chem. Phys. **89**, 3248 (1988).
[7] (a) A. Yoshimori, T. Kakitani, Y. Enomoto, N. Mataga, J. Phys. Chem. **93**, 8216 (1989). (b) Y. Hatano, T. Kakitani, Y. Enomoto, and A. Yoshimori, Mol. Simul. **6**, 191 (1991).
[8] (a) M. Tachiya, J. Phys. Chem. **93**, 7050 (1989). (b) M. Tachiya, *ibid.* **97**, 5911 (1993).
[9] K. Huang and A. Rhys, Proc. R. Soc. London, Ser. A **204**, 406 (1950).
[10] (a) R. A. Marcus, J. Chem. Phys. **43**, 1261 (1965). (b) N. S. Hush, Prog. Inorg. Chem. **8**, 391 (1967).
[11] (a) R. Englman and J. Jortner, Mol. Phys. **18**, 145 (1970). (b) N. R. Kestner, J. Logan, and J. Jortner, J. Phys. Chem. **21**, 2148 (1974). (c) M. Bixon and J. Jortner, Adv. Chem. Phys. **106**, 35 (1999).
[12] P. Chen and T. J. Meyer, Chem. Rev. **98**, 1439 (1998).
[13] (a) P. Chen, R. Duesing, D. K. Graff, and T. J. Meyer, J. Phys. Chem. **95**, 5850 (1991). (b) S. M. Hubig and J. K. Kochi, *ibid.* **99**, 17578 (1995). (c) N. Tétreault, R. S. Muthyala, R. S. H. Liu, R. P. Steer, J. Phys. Chem. A **103**, 2524 (1999).
[14] R. Kubo and Y. Toyozawa, Prog. Theor. Phys. **13**, 160 (1955).
[15] P. S. Reiseborough, Ann. Phys. **153**, 1 (1984).
[16] J. L. Skinner and D. Hsu, J. Phys. Chem. **90**, 4931 (1986).
[17] G. Fischer, *Vibronic Coupling* (Academic, London, 1984).
[18] (a) R. Islampour and S. H. Lin, J. Phys. Chem. **95**, 10261 (1991). (b) A. M. Mebel, M. Hayashi, K. K. Liang, and S. H. Lin, *ibid.* **103**, 10674 (1999).
[19] (a) T. Kakitani and N. Mataga, J. Phys. Chem. **89**, 8 (1985). (b) T. Kakitani and N. Mataga, *ibid.* **89**, 4752 (1985).
[20] (a) E. A. Carter and J. T. Hynes, J. Phys. Chem. **93**, 2184 (1989). (b) E. A. Carter and J. T. Hynes, J. Chem. Phys. **94**, 5961 (1991).
[21] M. Tachiya, Chem. Phys. Lett. **159**, 505 (1989).
[22] (a) S.-H. Chong, S. Miura, G. Basu, and F. Hirata, J. Phys. Chem. **99**, 10526 (1995). (b) S.-H. Chong and F. Hirata, J. Chem. Phys. **106**, 5225 (1997).
[23] (a) T. Ichiye, J. Chem. Phys. **104**, 7561 (1996). (b) R. B. Yelle and T. Ichiye, J. Phys. Chem. B **101**, 4127 (1997).
[24] Y. Georgievskii, J. Chem. Phys. **104**, 5251 (1996).
[25] H.-X. Zhou and A. Szabo, J. Chem. Phys. **103**, 3481 (1995).
[26] (a) A. Yoshomori, Chem. Phys. Lett. **184**, 76 (1991). (b) T. Fonseca and B. M. Ladanyi, J. Mol. Liq. **60**, 1 (1994). (c) P. van der Meulen, A. M. Jonkman, and M. Glasbeek, J. Phys. Chem. A **102**, 1906 (1998).
[27] D. V. Matyushov and B. M. Ladanyi, J. Chem. Phys. **110**, 994 (1999).
[28] Static and dynamic solvent responses both increasingly deviate from the linear response regime with decreasing solvent density. The linear response approximation breaks down for supercritical solvent densities, see (a) M. Re and D. Laria, J. Phys. Chem. B **101**, 10494 (1997). (b) P. Graf and A. Nitzan, Chem. Phys. **235**, 297 (1998). (c) T. Yamaguchi, Y. Kimura, and N. Hirota, J. Chem. Phys. **111**, 4169 (1999).
[29] Substantial nonlinearity has been reported for the ET reorganization entropy, see L. W. Ungar, M. D. Newton, and G. A. Voth, J. Phys. Chem. B **103**, 7367 (1999). The entropies of charge separation and charge recombination were also found to be different due to nonlinear solvetion effects, see Ref. 38b.
[30] Nonparabolic free energy surfaces have been observed in simulations of heterogeneous ET, see J. B. Straus, A. Calhoun, and G. A. Voth, J. Chem. Phys. **102**, 529 (1995).
[31] D. V. Matyushov and G. A. Voth, J. Phys. Chem. **104**, ■■■ (2000) (in press).
[32] (a) A. J. Leggett, S. Chakravarty, A. T. Dorsey, M. P. A. Fisher, A. Garg, and W. Zwerger, Rev. Mod. Phys. **59**, 1 (1987); (b) A. Garg, J. N. Onuchic, and V. Ambegaokar, J. Chem. Phys. **83**, 4491 (1985).
[33] (a) F. O. Raineri, B. C. Perng, and H. L. Friedman, Z. Phys. Chem. **204**, 109 (1998); (b) F. O. Raineri and H. L. Friedman, Adv. Chem. Phys. **107**, 81 (1999).
[34] M. D. Newton, Adv. Chem. Phys. **106**, 303 (1999).
[35] I. S. Gradshteyn and I. M. Ryzhik, *Table of Integrals, Series, and Products* (Academic, San Diego, 1994).
[36] Zhou and Szabo (Ref. 25) suggested an approximate relation $\Delta F_0 = \hbar\omega_m + \Delta\lambda/6$ based on a truncated polynomial expansion of $\mathcal{F}_i(\xi,0)$ in powers of ξ.

[37] (a) P. F. Barbara, T. J. Meyer, M. A. Ratner, J. Phys. Chem. **100**, 13148 (1996); (b) K. Ando and J. T. Hynes, Adv. Chem. Phys. **110**, 381 (1999).
[38] (a) R. F. Loring, J. Phys. Chem. **94**, 513 (1990); (b) D. V. Matyushov and B. M. Ladanyi, J. Chem. Phys. **107**, 1375 (1997).
[39] A comparison of the reorganization energies for polarizable (Table III) and nonpolarizable (Table II) dipolar hard spheres demonstrates their very little sensitivity to the solvent polarizability. This feature has been noticed previously, see P. Vath, M. B. Zimmt, D. V. Matyushov, and G. A. Voth, J. Phys. Chem. B **103**, 9130 (1999).
[40] The third cumulant is identically zero in perturbation solvation theories employing the unperturbed dipolar solvent as the reference system. It is, however, nonzero in reality due to a solute-induced change in the solvent structure. The fact that the third cumulant $\beta^3\langle(\delta X)^3\rangle_2/6$ is about an order of magnitude smaller than the second cumulant $\beta^2\langle(\delta X)^2\rangle_2/2$ (Table II) is an indication that the solute does not modify dramatically the solvent structure and the unperturbed solvent is a good zeroth-order approximation.
[41] We do not report the third cumulants in Table III because of their substantial dependence on the number of particles in the simulation box. For instance, $\beta^3\langle(\delta X)^3\rangle_2$ drops from 14.4 to 10.8 when switching from $N=256$ to $N=500$ at $\alpha_0^*=0.05$, $\alpha^*=0.05$, and $\Delta m_0/m=8.0$.
[42] The quadratic in the nuclear polarization term $(\Delta\tilde{\alpha}/2)\mathbf{R}_p^2$ breaks the linear dependence of X on $\mathbf{R}_p$. The free energy surface then loses its symmetry with respect to the transformation $X\rightarrow -X$ for the charge-neutral state with $m_{01}=0$ in opposite to the case of $\Delta\alpha=0$ (Ref. 7).
[43] For some reactions involving photoexcited initial states, e.g., primary charge separation in photosynthetic reaction centers, the polarizability change is negative [D. S. Gottfried, M. A. Steffen, S. G. Boxer, Biochim. Biophys. Acta **1059**, 76 (1991)]. The nonlinear solvation and polarizability effects then add up.
[44] (a) G. U. Bublitz and S. G. Boxer, Annu. Rev. Phys. Chem. **48**, 213 (1997); (b) F. W. Vance, R. D. Williams, and J. T. Hupp, Int. Rev. Phys. Chem. **17**, 307 (1998).
[45] Stark measurements in condensed phases may be not a very reliable source of the vacuum polarizability variation $\Delta\alpha_0$ or the parameter $\Delta\tilde{\alpha}$ considered here. This is because the field-induced orientation of the probe molecule and/or of the polar groups in the matrix make a substantial effect on the measured $\Delta\alpha_0^{\mathrm{Stark}}$. Furthermore, the ability of the solute and/or solvent molecules to reorient on the time scale of the Stark measurement can affect the measured polarizability change by up to two orders of magnitude, see A. Chowdhury, D. A. Locknar, L. L. Premvardhan, and L. A. Peteanu, J. Phys. Chem. A **103**, 9614 (1999).
[46] E. Lippert, V. Bonačič-Koutecký, F. Heisel, and J. A. Miehé, Adv. Chem. Phys. **68**, 1 (1987).
[47] In order to simplify the discussion, we have not considered here the modulation of I_i by fluctuations of Q. This term appears due to the solvation free energy by the electronic polarization of the solvent entering I_i, see D. V. Matyushov, Chem. Phys. Lett. **203**, 131 (1993).
[48] D. Gust, T. A. More, and A. L. More, Acc. Chem. Res. **26**, 198 (1993).
[49] (a) F. J. Vesely, J. Comput. Phys. **24**, 361 (1977); (b) G. N. Patey, G. M. Torrie, and J. P. Valleau, J. Chem. Phys. **71**, 96 (1979); (c) C. Kriebel and J. Winkelmann, Mol. Phys. **88**, 559 (1996).
[50] M. P. Allen and D. J. Tildesley, *Computer Simulation of Liquids* (Clarendon, Oxford, 1987).